Compatibilizing and toughening blends of recycled acrylonitrile-butadiene-styrene/recycled high impact polystyrene blends via styrene-butadiene-glycidyl methacrylate terpolymer

Xiangning Meng,[a] Yingchun Li,[a,*] Najla AlMasoud,[b] Wensheng Wang,[a] Taghrid S. Alomar,[b] Jie Li,[a] Xinming Ye,[a] Hassan Algadi,[c,d,f] Ilwoo Seok,[e,*] Handong Li,[f] Ben Bin Xu,[f,*] Na Lu,[h] Zeinhom M. El-Bahy,[g] and Zhanhu Guo[f,*]

[a] School of Materials Science and Engineering, North University of China, Taiyuan, China

[b]Department of Chemistry, College of Science, Princess Nourah bint Abdulrahman University, P.O. Box 84427, Riyadh 11671, Saudi Arabia

[c] College of Materials Science and Engineering, Taiyuan University of Science and Technology, Taiyuan 030024, China

[d] Department of Electrical Engineering, Faculty of Engineering, Najran University, Najran 11001, Saudi Arabia

[e] Mechanical Engineering, Arkansas State University, PO Box 1740, State University, AR, 72467, USA

[f] Mechanical and Construction Engineering, Faculty of Engineering and Environment, Northumbria University, Newcastle Upon Tyne, NE1 8ST, UK

[g] Department of Chemistry, Faculty of Science, Al-Azhar University, Nasr City 11884, Cairo, Egypt

[h] Lyles School of Civil Engineering, Purdue University, West Lafayette, IN 47907-2051, USA

*Corresponding author:

E-mail address*: liyingchun@nuc.edu.cn (Y. Li), iseok@astate.edu (I Seok), ben.xu@northumbria.ac.uk (B. Xu); zhanhu.guo@northumbria.ac.uk (Z. Guo)

ABSTRACT

To increase the effectiveness of recovered acrylonitrile-butadiene-styrene (rABS) and recycled high impact polystyrene (rHIPS), styrene-butadiene-glycidyl methacrylate (SBG) was incorporated to the rABS/rHIPS system by melt blending for the first time. Multiple epoxy groups in SBG can combine with the butadiene ageing groups in rABS/rHIPS to generate ester groups, repairing the broken molecular chains, improving the compatibility between the two phases, and enhancing the mechanical properties of the blends. The findings demonstrated that adding SBG greatly increased the blends' molecular weight, impact strength, tensile strength, flexural strength, storage modulus, loss modulus, and complex viscosity. When SBG content was 8 wt%, the notch impact strength of the blends reached 8.84 kJ/m^2, which was 108% higher than that of rABS/rHIPS. In addition, the interface between polybutadiene (PB) phase and styrene-acrylonitrile copolymer (SAN) phase became more blurred, and the compatibility of the two phases was improved, which enabled the high-value recovery of rABS/rHIPS.

Keywords: acrylonitrile-butadiene-styrene; high impact-resistance polystyrene; toughening.

1. Introduction

The increasing consumer desire for electronic devices [1-5] has significantly accelerated one of the world's fastest growing waste streams, namely the waste electrical and electronic equipment (WEEE), due to the rapid development of materials [6-15] and electronics [16-22]. Poor WEEE handling will lead to a significant buildup of waste plastic in the environment [23-27]. The plastic waste may experience aging, fracture and migration, as a result, it becomes a major source of microplasticity, which not only poses a threat to human health, but also causes damages to the natural environment [28, 29]. Moreover, the amount of WEEE will continue to increase due to the increasing demand for electronic products and the regular renewal of equipment, with more than 74.7 million tons of electronic waste reportedly generated worldwide by the end of 2030, with a per capita production of 9 kg [30-32]. In WEEE, polymers account for about 10-15% [33]. Numerous thermosetting and thermoplastic plastics, including polycarbonate (PC), polyamide (PA), polypropylene (PP), polystyrene (PS), high impact polystyrene (HIPS), and others, are present in it. The majority is made up of ABS and HIPS [34-37].

ABS is a typical engineering polymer, which includes rubber dispersed phase (PB) and amorphous continuous phase (SAN) [38]. The PB phase makes it have high elasticity and toughness, while the SAN phase affects its processing properties, heat resistance, chemical resistance and surface hardness [39, 40]. Because of these qualities, ABS is frequently used in a variety of sectors, including those related to machinery, electrical, textile, cars, airplanes, and ships [41]. High impact toughness, fluidity, gloss, and heat resistance characterize HIPS, a thermoplastic

substance composed of elastomer-modified polystyrene [42]. It has been widely applied in industry, mainly used in household appliances, construction, instruments, toy housing, and material packaging industries [43, 44].

The chemical composition and structure of polymer materials will change over time as a result of the extensive impacts of environmental variables such as heat, oxygen, water, light, microorganisms, chemical media, etc. [45]. ABS plastic and HIPS plastic are easy to age in natural environment. The main reason for aging is the PB phase in the structure [46]. Under the action of oxygen, the (C=C) bonds in PB phase generate hydroperoxides, which continue to be decomposed and generate oxygen-containing groups such as carbonyl, carboxyl, and hydroxyl groups [47, 48]. Finally, phase separation occurs inside the plastic and the compatibility is deteriorated [49-51]. ABS and HIPS not only are the two polymers with the most content in WEEE, but also have similar density. ABS/HIPS blends are immiscible and exhibit a complex morphology, despite the fact that both contain PS and polybutadiene (PB), which has a direct impact on the material's mechanical and rheological behavior [33, 52]. Therefore, it is an effective way to improve the utilization efficiency of waste plastics to recycle the blends of recycled ABS (rABS) and recycled HIPS (rHIPS) [53]. At present, there are few ways to modify ABS/HIPS blends. For example, Denise Hirayama *et al*. improved the performance of the blends by adding compatibilizer SEBS/SBS and ABS/HIPS blends to rABS/rHIPS [54]. Vazquez et al. added styrene butadiene rubber to rABS/rHIPS to enhance the composites' mechanical characteristics. The findings revealed that the strength and toughness of the blends increased by 244% and 186%, respectively, when the addition

amount of SBR was 2 wt% [55].

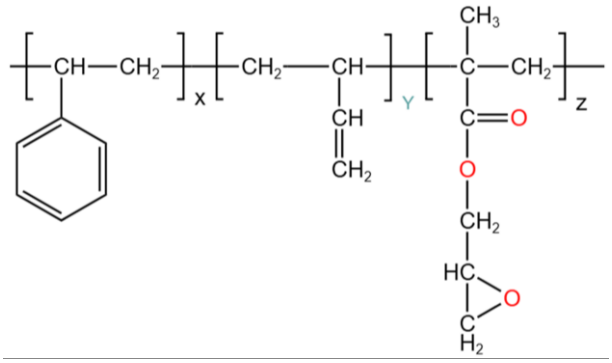

Fig. 1. The chemical formula of SBG.

In this study, SBG was added to rABS/rHIPS blends for the first time. On one hand, SBG is a terpolymer and the structural formula is shown in **Fig. 1**, where "S" (styrene) and "B" (butadiene) are also common structures of rABS/rHIPS, so SBG offers significant benefits enhancing the compatibility of the blends [56]. At the same time, "G" glycidyl methacrylate contains an active group, epoxy group, which can react with the matrix. The epoxy group can react with the aging group and play the role of chain expansion, so as to improve the impact resistance of the composite [57-59]. On the other hand, SBG is a core-shell structure compatibilist, with PB phase as the core, and its surface covered with a layer of highly active epoxy groups. Therefore, SBG can not only effectively improve the compatibility of rABS/rHIPS, but also enhance their toughness [60].

This research aimed to investigate the impact of SBG on rABS/rHIPS performance. Through the use of Fourier transform infrared spectroscopy (FTIR), gel permeation chromatography (GPC), rotational rheological testing, differential scanning calorimetry (DSC), dynamic mechanical analysis (DMA), scanning electron microscopy (SEM), mechanical property testing, and

thermogravimetric analysis, the chemical structure, molecular weight, mechanical properties, dynamic mechanical properties, rheological properties, and morphology of the modified products were investigated (TG). The mechanical characteristics and compatibility of rABS and rHIPS blends were both enhanced.

2. Experimental

2.1. Materials

The rABS and rHIPS were kindly supplied by Yangzhou Ningda Precious Metals Co., Ltd. (Jiangsu China). SBG was obtained from Jia Yi Rong Polymer Co., Ltd. (Shanghai, China). No treatments were applied to any of the chemicals, they were used as received.

2.2. Preparation of the rABS/rHIPS/SBG blends

The rABS, rHIPS, and SBG were dried in an electric thermostatic drying kiln at 80 °C for 8 hours (DHG-9070A, Yuhua Industrial Co., Ltd. Hangzhou, China) before processing. The blends were reactively extruded through a 36 mm co-rotating twin-screw extrude (TNS-35D, Nanjing Ningping Extrusion Machinery Co. Ltd, Nanjing, China). The extruder's operating temperature ranged between 195 and 225°C, and its rotational speed was 80 rpm. The blends were injected into a mould using an injection moulding machine (JH600, Weidaliyuan Machinery Co. Ltd, Zhangjiagang, China), before being dried in an electric thermostatic oven at 80℃ for 8 h. The temperature of injection-molding machine was in the range of 200-220℃. The injection molding machine can inject three kinds of samples at one time, among which the dumbbell type is used to test the tensile strength of the material, the rectangular type is used to test the notched impact

strength and flexural strength, and the bar type is used to test the melt index. The accurate formulations are summarized in **Table 1**.

Table 1. Compositions of the modified samples in this study.

Sample	rABS/rHIPS (wt%)	SBG (wt%)
1	60/40	0
2	58.8/39.2	2
3	57.6/38.4	4
4	56.4/37.6	6
5	55.2/36.8	8
6	54/36	10

2.3. Characterizations

2.3.1 Fourier transform infrared spectroscopy (FTIR)

The FTIR spectra were carried out with a Tensor-27 instrument (Bruker, Ettlingen, German) in the wavenumber range 4000–500 cm^{-1}, and the resolution was 4 cm^{-1} over 32 scans at room temperature. The rABS, rHIPS and SBG were dried at 80°C for 8 h and KBr was dried at 120°C for 6 hours before testing. The sample was them pressed with KBr under the infrared baking lamp, and the mass ratio of KBr to the sample was approximately 100:1.

2.3.2 Gel permeation chromatography (GPC)

GPC was used with a gel permeation chromatography instrument to calculate the number-average molecular weight (Mn), weight-average molecular weight (Mw), and polydispersity index

(PDI) of rABS/rHIPS/SBG mixtures (Waters 515, Waters Corporation, Milford, USA). Tetrahydrofuran was used as an eluent (flow rate 1.0 mL/min) at 35℃. All the samples were prepared as 3.5 mg/mL solutions in tetrahydrofuran, with approximately 60 μL sample being injected into GPC. Polystyrene standards were followed to calibrate the molecular weight.

2.3.3 Rheological characterization

The oscillatory rheological evaluation of these samples was carried out at 190℃ on a BohlinCVO150 rheometer (Malvern Instruments, Ltd., United Kingdom) with a 25 mm parallel circular arrangement. Before characterization, the materials were dried in an oven at 80℃ for 8 h. A frequency of 1–100 rad/s and a strain amplitude of 1% were used during the measurement to guarantee that all of the samples' characterizations were in the linear viscosity area.

2.3.4 Melt flow index (MFI)

MFI was determined with a melt flow indexer (ZRZ1452, MTS STSTEMS Co., Ltd., China) with a loading of 2.16 kg at 220℃. MFI samples were dried in vacuo at 80℃ for 8 h.

2.3.5 Differential scanning calorimetry (DSC)

The blends were evaluated with a differential scanning calorimeter (DSC 3, Mettler-Toledo Instruments (Shanghai) Co., Ltd. The samples used were ranging between 5-8 mg in weight. They were initially heated (25–200℃ at 10℃/min) followed a by cooling process (200–25℃ at 10℃/min) in order to remove the thermal history, and once again heated (25–160℃ at 10℃/min). The second heating procedure yielded the glass transition temperature (Tg) number. Tests were carried out in a nitrogen environment with a 50 mL/min flow rate.

2.3.6 Dynamic mechanical analysis (DMA)

DMA was performed under the small stretching mode with a DMA SDTA861e instrument (Mettler-Toledo, Switzerland) at a frequency of 1 Hz with sample dimensions of 20 × 4 × 2 mm^3. The samples were measured in the temperature range 25-160℃ at a heating rate of 5℃/min.

2.3.7 Scanning electron microscopy (SEM)

In order to produce a better contrast, two kinds of fracture surfaces were selected for testing. The first is low-temperature fracture, where the sample is first frozen in liquid nitrogen for four hours and then interrupted with the pendulum of impact testing, and the second is the sample fracture surface after impact testing at room temperature. Both fracture surfaces were sprayed with gold for better imaging.

2.3.8 Mechanical property tests

Tensile strength and flexural strength were measured using a universal testing machine (AL-7000M, Gotech Testing Machines Co. Ltd, Guangdong, China) at room temperature. Tensile strength test was conducted according to GB/T 10440.1-2018 standard. Dumbbell type II was used for the sample, with a standard distance of 25 mm and a tensile speed of 50 mm/min. The bending strength test was carried out according to GB/T 9341-2008 standard with a distance of 64 mm and a falling speed of 10 mm/min. The XJU-22 impact testing machine (Kebiao Testing Machines Co., Ltd. Chengde, China) was used to determine the notched impact strength in terms of GB/T 1043–2008 under ambient temperature. First, the impact spline was made a notch of 45° on the notched machine, and the stress was relaxed for 24 h at room temperature. Then, the impact test was carried

out on the cantilever beam impact testing machine. At least ten samples were tested in each test, and the average values were recorded.

2.3.9 Thermogravimetric analysis (TGA)

The thermogravimetric analysis (TGA) was used to examine the products' thermal stability. The nitrogen rate was 20 mL/min, and the sample mass was approximately 5 mg. The heating pace was 10°C/min, and the temperature range was 30-600°C.

2. Results and discussion

3.1. FTIR Spectral Analysis

Fig. 2 (a) shows the FTIR spectra of SBG, virgin ABS, virgin HIPS, rABS and rHIPS. At 966 cm^{-1} and 906 cm^{-1} are the in-plane bending vibration characteristic peaks of trans-1, 4-butadiene and the out-of-plane bending vibration characteristic peaks of cis-1, 2-butadiene, respectively. The infrared characteristic peaks at 757cm^{-1} and 701 cm^{-1} are the out-of-plane deformation vibrations absorption peaks of the single substituted benzene ring. The above are the basic characteristic peaks of PS and PB, which are a common part of the three raw materials. A strong C=O stretching vibration peak was found near 1730cm^{-1}, which was the basic characteristic peak of glycidyl methacrylate in SBG. The peak of nitrile group is about 2237 cm^{-1}, which is the basic characteristic peak of ABS [61]. It can be found from the infrared spectrum of rABS and rHIPS that, compared with the new material, the spectrum has a wider stretching vibration peak at 3438 cm^{-1}. The absorption peak is the stretching vibration peak of the free hydroxyl group in the carboxyl group, which is the result of aging. **Fig. 2** (b) shows the FTIR spectrum of rABS/rHIPS/SBG blend.

Compared with the spectrum of the original material, FTIR spectrum of rABS/rHIPS blend shows a more obvious carbonyl vibration peak at 1730 cm^{-1}. This suggests that the (C=C) bonds in PB are broken by air or light, forming oxygen-containing compounds such as carboxyl groups[62].

After the addition of SBG, a new ether group peak was generated at 1069 cm^{-1}, indicating that the epoxy group on the SBG reacted with the carboxyl group and hydroxyl group produced after the aging of the polymer to form ether group. The possible reactions are shown in **Fig. 3.**

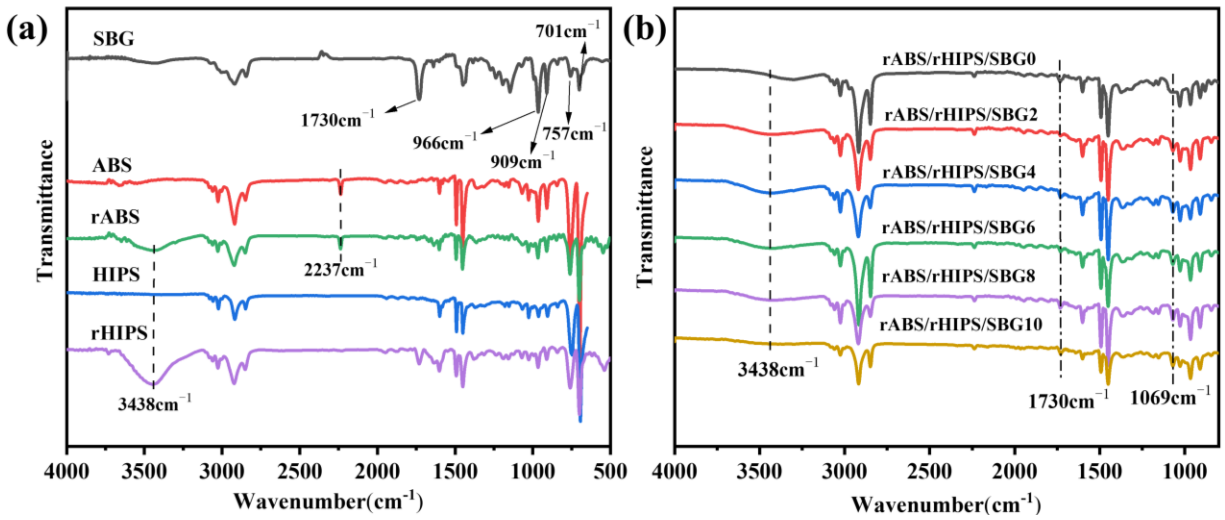

Fig. 2. FTIR spectra of SBG, virgin ABS, virgin HIPS and rABS/rHIPS/SBG blends.

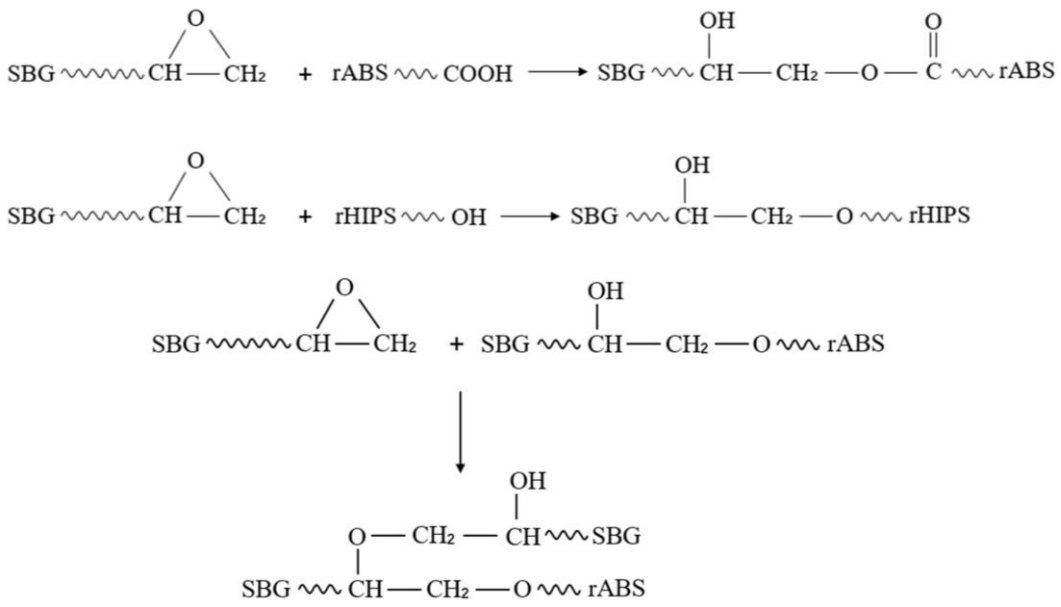

Fig. 3. Schematic of compatibilization reaction mechanism.

3.2. Determination of molecular weight

GPC is mainly used to determine the relative molecular mass and distribution of polymer materials. When the dilute polymer solution passes through the porous gel stationary phase, the large polymer cannot enter the gel cavity, but can only pass through the column along the gap between the porous gel particles and be eluted out by the mobile phase. **The** number average molecular weight (Mn), weight average molecular weight (Mw) and polydispersity Index (PDI) of rABS/rHIPS blends with different SBG contents are shown Table 2. The figure shows that Mn and Mw of the blend were positively correlated with the SBG content, which indicated that the epoxy group on the SBG had a strong ability to link molecular chains. It acts as a bridge, reconnecting aging molecular chains to achieve the enhanced polymer properties. The molecular weight distribution of polymers, and its value is equal to the ratio of Mw to Mn. As the SBG content kept on increasing , the PDI of the blends was decreased, indicating that the molecular weight

distribution of the matrix became more and more uniform [63].

Table 2.GPC results of rABS/rHIPS/SBG blends.

Specimen	Mn	Mw	PDI
rABS/rHIPS/SBG0	7085	53975	7.62
rABS/rHIPS/SBG2	10902	53552	4.91
rABS/rHIPS/SBG4	11793	56796	4.82
rABS/rHIPS/SBG6	13057	56014	4.29
rABS/rHIPS/SBG8	14314	58830	4.11
rABS/rHIPS/SBG10	15294	62555	4.09

3.3. Rheological properties

Polymer melt has a unique dynamic fluidity due to its chain-like development structure. Understanding its fluidity is very important for the analysis of polymer structure and compatibility [64]. It can be seen in **Fig. 4** (a) and (b), the G ' and G " of rABS/rHIPS/SBG blends increase significantly with increasing the frequency. This is because in the low frequency region, the deformation of the molecular chain can keep up with the changes in the external force, so G ' and G " are lower. The acting period of shear force decreases as frequency increases, that is, the deformation time of macromolecular chain becomes shorter, which is far less than the relaxation time of molecular chain. This results in the deformation of the macromolecular chains, which cannot keep up with the changes of external forces, resulting in the elastic properties of the system, so that G ' increases considerably [65]. The friction resistance of the material to overcome the

movement of the chain segment in unit time and the energy loss of the system both increase concurrently with an increase in shear frequency, and as a result, the G " also increases considerably.

Fig. 4 (a) and (b) shows that the G ' and G " of the blends added with SBG are larger than those of the original blends. The modulus of the blends at low frequencies increased with the inclusion of SBG, which was attributed to the improved compatibility of rABS and rHIPS. Lyu *et al*. [66] also reported similar results, the modulus in the low-frequency region increases with the enhancement of the two-phase interaction. The melt flow behavior of polymer is not a simple relative slip between polymer chains, but the total result of the motion unit transition in turn. When an outside force acts on a polymer chain, it will undoubtedly extend in that direction, and the polymer chain will spontaneously curl up when the external force is removed. The addition of SBG enhances the interaction between SBG and polymer matrix, hinders the movement of molecular chains, and makes the conformational change more complex. Under the action of external forces, more energy can be absorbed.

Fig. 4(c) shows the curve of complex viscosity of rABS/rHIPS/SBG blends as a function of angular frequency at 190 °C. It can be seen that as the angular frequency rises, the polymer's complex viscosity diminishes which is a typical shear thinning phenomenon. This is due to the fact that under the influence of high shear frequency, disentanglement outweighs tangling,, the internal network structure of the system dissolves, the viscosity decreases, and the phenomenon of shear thinning occurs. The epoxy groups in SBG may have reacted with the carboxyl and hydroxyl groups in rABS/rHIPS to raise the complex viscosity of the blends as the SBG content was

increased.. SBG reconnected the broken molecular chains, increasing the molecular weight and entangling between the molecular chains. The increase of the complex viscosity of the blends also directly indicated the compatibility of the polymer. The two-phase dispersion of the polymer is very sufficient. This dispersion state can make the interface of the two phases have a strong interaction, and the flow resistance of the blends increases, so the viscosity increases.

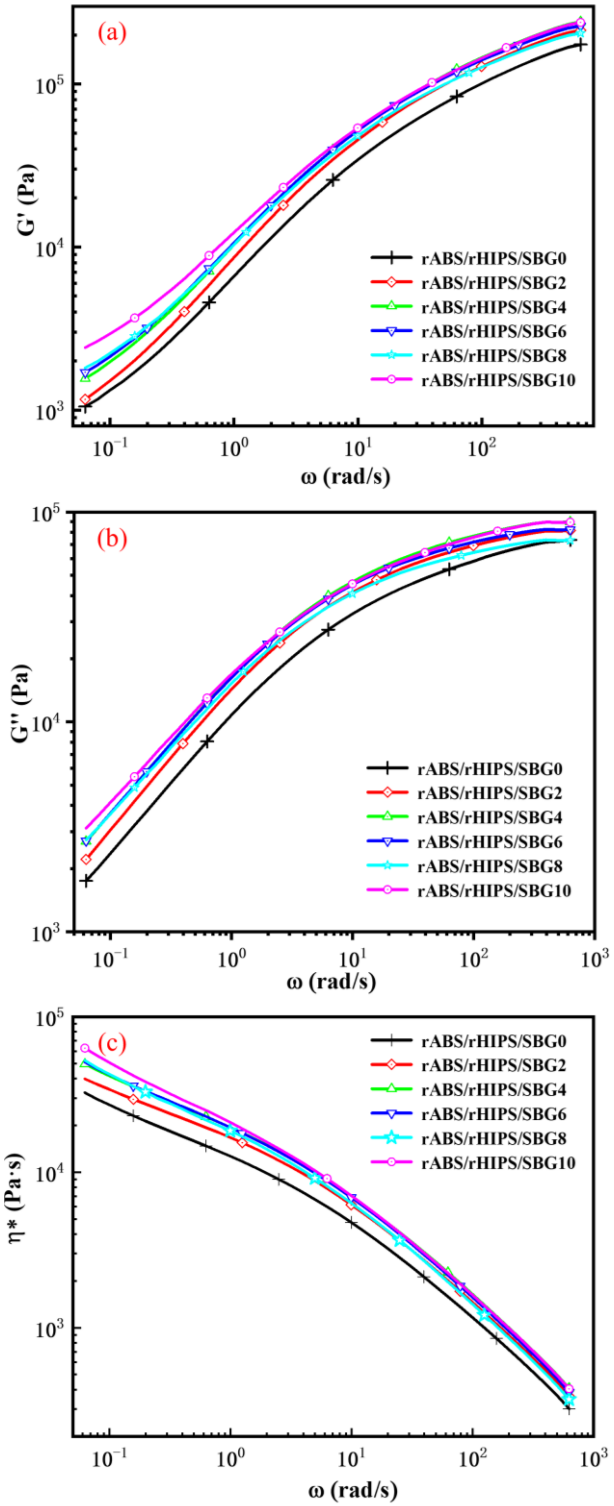

Fig. 4. Rheological property versus frequency for rABS/rHIPS/SBG at 190 °C: (a) G ', (b) G ", (c) η*.

3.4. Melt flow behavior

MFI can reflect the flowability of the material during processing, and the molecular structure of the blends can be analyzed in conjunction with the polymer rheological properties mentioned above. **Fig. 5** is the MFI of the blends with different SBG contents. The MFI of the blends considerably decreased as the SBG content increased, and the addition of SBG made the flow of the blends worse, indicating that SBG reacted with the matrix, resulting in the increase of molecular entanglement, which restricted the flow of the polymer. This agrees with the GPC test findings mentioned above.

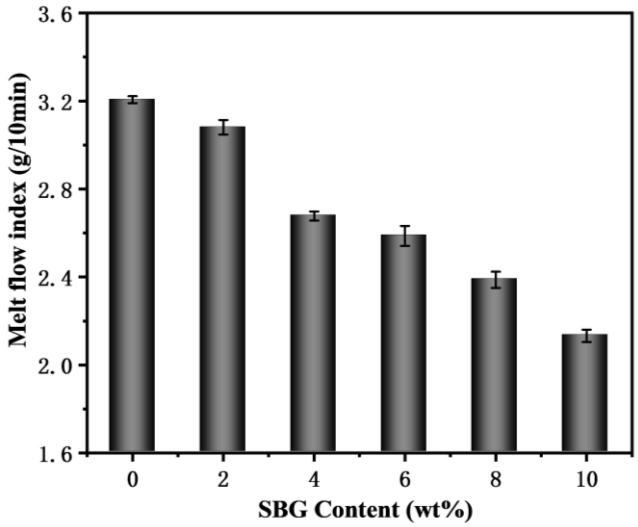

Fig. 5. MFI of the rABS/rHIPS/SBG blends.

3.5. Differential Scanning Calorimetry (DSC)

The DSC curve gives the T_g of the sample and is used to assess the blends' compatibility [67]. **Fig. 6** shows the DSC curves of rABS/rHIPS blends with different SBG contents. From left to right, the first peak of each curve corresponds to the T_g of the PS phase in HIPS and the second

peak corresponds to the T_g of the SAN phase in ABS. As can be seen from **Fig. 6**, the T_g of the blends tends to be close to each other with the continuous increase of SBG content, which further indicates that the compatibility of the blends has been improved. At the same time, the T_g of PS phase gradually increased from 102.23℃ to 106.96℃, and that of SAN phase gradually increased from 128.19℃ to 128.68℃. The T_g of the blends with different SBG contents are listed in **Table 3**. The reason why the T_g moves to the high temperature region may be due to the reaction between epoxide group and carboxyl group. The reason for T_g moving to the high temperature region may be that the reaction between the epoxy group and the aging group increases the molecular weight of the polymer, which limits the movement of the polymer chain segments.

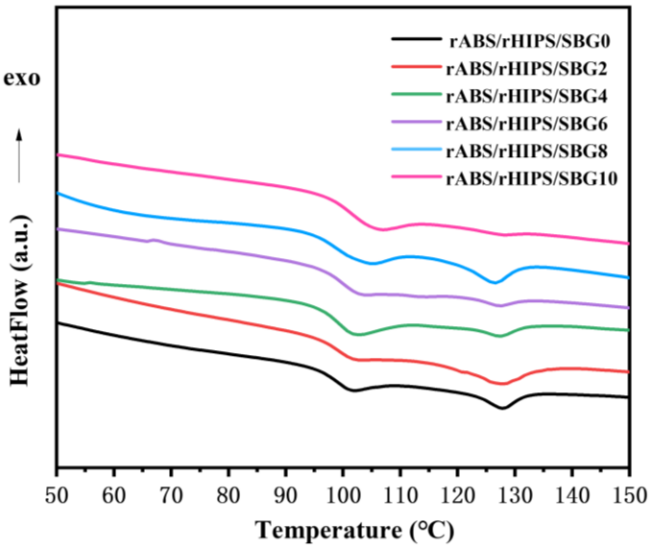

Fig. 6. DSC of the rABS/rHIPS/SBG blends during the reheating process.

Table 3. Glass transition temperature of rABS/rHIPS/SBG blends.

Sample	PS (℃)	SAN (℃)	$\triangle T_g$ (℃)
rABS/rHIPS/SBG0	102.23	128.19	25.96
rABS/rHIPS/SBG2	102.72	127.65	24.93
rABS/rHIPS/SBG4	102.73	127.71	24.98
rABS/rHIPS/SBG6	103.71	127.68	23.97
rABS/rHIPS/SBG8	104.70	126.66	21.96
rABS/rHIPS/SBG10	106.96	128.68	21.72

3.6. Dynamic mechanical analysis (DMA)

The compatibility and interplay between rABS, rHIPS, and SBG were assessed using the DMA tests.. The storage modulus curves of rABS/rHIPS and rABS/rHIPS/SBG8 are shown in **Fig. 7** (a). Storage modulus refers to the amount of energy stored due to elastic deformation when a material is undergoing an elastic deformation, which reflects the elastic properties of the material. **Fig. 7** (a) illustrated, the storage modulus was improved when 8% SBG was added to the blends. This indicates that the modified material has a good elasticity and strong ability to restore the original deformation after removing the stress. This may be caused by the increase of molecular chain entanglement during melting and blending, which leads to the improvement of material properties.

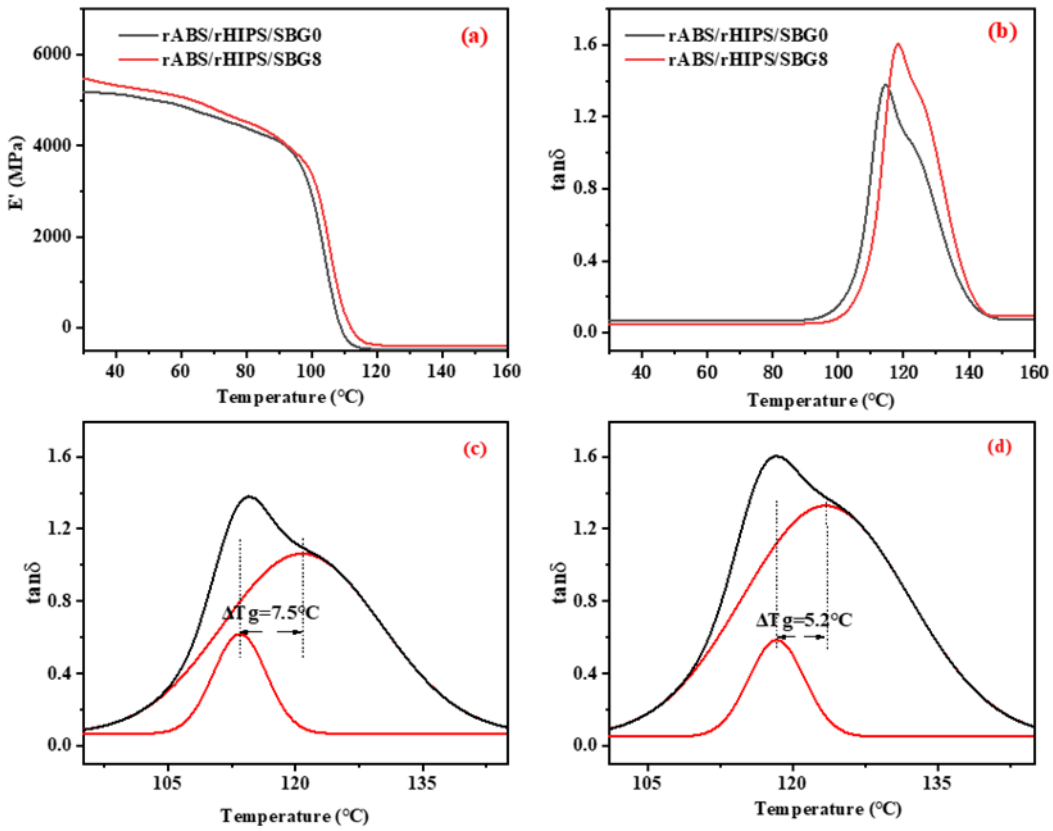

Fig. 7. Storage modulus (a) curves of rABS/rHIPS/SBG blends; tanδ (b) curves of rABS/rHIPS/SBG blends. After peak fitting treatment :(c) the unmodified sample (rABS/rHIPS/SBG 0) and (d) the modified sample (rABS/rHIPS/SBG 8).

The tanδ curves of rABS/rHIPS and rABS/rHIPS/SBG8 are shown in **Fig. 7** (b). When studying the damping materials, the temperature corresponding to the peak value in the tanδ curve is often regarded as the T_g [68]. It is evident from the figure that the glass transition temperature of the blends increases after SBG is added. In order to better obtain the changing trend of T_g , the curve in the figure is processed by peak fitting, and the result can be seen in **Fig. 7** (c) (d). It is also noticeable from the **figure** that the curve is divided into two peaks of the curve, from left to right,

the first peak belongs to the T_g of the PS phase in HIPS, and the second peak to the T_g of the SAN phase in ABS. On one hand, the T_g of both phases move to the high temperature region after the addition of SBG. On the other hand, the T_g of SAN phase and PS phase are close to each other. The results are shown in **Table 4.** In dynamic mechanical analysis, if the two polymers are partially compatible, the T_g of the blends will be close to each other. This is in line with the testing findings of the earlier DSC test.

Table 4. Glass transition temperature of rABS/rHIPS/SBG0, rABS/rHIPS/SBG8.

Sample	PS (℃)	SAN (℃)	$\triangle T_g$ (℃)
rABS/rHIPS/SBG0	113.5	120.9	7.5
rABS/rHIPS/SBG8	118.3	123.5	5.2

3.7. Morphological analysis

SEM is frequently used to examine the distribution and structure of each polymer phase especially for the study of surface morphology [69, 70]. **Fig. 8** (a) and (b) show the morphology of the blends after fracture at low temperature at 5000 magnifications. Looking back to **Fig. 8** (a) it can be seen that many holes are dispersed in the matrix, which is caused by the extraction of rubber phase in the blends. Additionally, the interface between the continuous phase and the dispersed phase is plainly visible,, which indicates that the compatibility between rABS and rHIPS is poor. Compared with **Fig. 8** (a), the interface between the distributed phase and the continuous phase in **Fig. 8** (b) becomes blurred and there is no obvious interface, which indicates that the compatibility of rABS and rHIPS has been significantly enhanced after the addition of 8% SBG.

Fig. 8 (c) and (d) are the impact fracture morphology of the blends at 5000 magnifications. Many layered structures can be seen in **Fig. 8** (c), which reflects the poor compatibility between rABS and rHIPS[71]. In contrast, such layered structures almost disappear in **Fig. 8** (d), which indicates that the compatibility between rABS and rHIPS has become better. Moreover, more spherical structures than **(c)** can be clearly seen in the figure, indicating that the addition of SBG not only supplements the absence of rubber phase, but also makes the rubber phase more evenly dispersed in the matrix, which will be crucial in enhancing the blends' toughness. **Fig. 8** (e) and (f) show the impact fracture morphology of the blends at 2000 magnifications. Different from (c) and (d), the sampling point of this time selects the surface morphology far from the gap, and the surface morphology in this region shows a state like that of tearing. It can be seen that the layered structure in **Fig. 8** (f) is much less than that in **Fig. 8** (e), which is consistent with the effect presented in **Fig. 8** (c), (d) and more obvious. In conclusion, the three fracture patterns showed that the compatibility and toughness of rABS and rHIPS were improved by the inclusion of SBG.

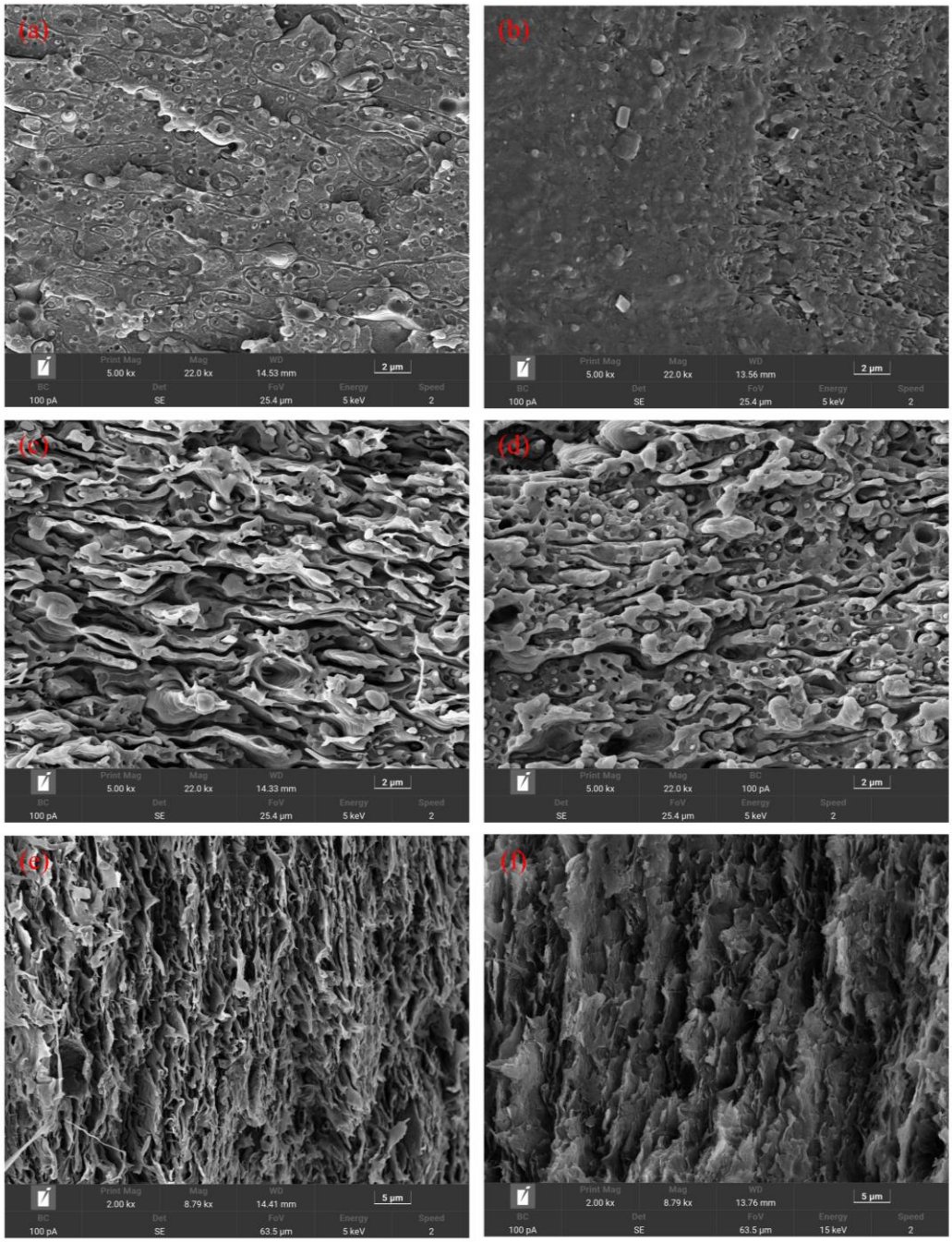

Fig. 8. SEM of samples: (a)，(c)，(e)：the unmodified sample (rABS/rHIPS) and (b)，(d)，(f)：modified sample (rABS/rHIPS/SBG 8).

3.8. Mechanical properties analysis

Fig. 9 (a) shows the results of notched impact strength and tensile strength of rABS/rHIPS/SBG blends. The black line in the figure shows how the blends' notched impact strength rises at first, then decreases. When the content of SBG is 8 wt%, the notched impact strength of the blends reaches the maximum value of 8.84 kJ/m^2, which is 108% higher than that of the blends without SBG. On the other hand, the PB phase in SBG plays a very crucial role as an elastomer in enhancing impact strength. When the sample is impacted, the elastomer particles act as stress concentration points, creating a large number of crazes, which can absorb more energy. However, when the SBG content exceeds 8%, the notch impact strength of the blend decreases, which may be due to excessive cross-linking in the matrix restricting the movement of molecular chains.

Fig. 9 (b) shows the stress-strain curves of rABS/rHIPS/SBG blends. The rABS/rHIPS blends show a very low elongation at break, and the material is characterized by its hardness and brittleness. The slope of the curve increases after the addition of SBG, which indicates that the Young's modulus of the blends increases, and the elongation at break of the blends also keeps increasing. When the content of SBG reached 8%, the elongation at break of the blends increased to 32.6%, which may be due to the improvement of compatibility and the increase of the elongation at break. At this time, the blends show strong and tough characteristics. Similarly, the area of the stress-strain curve can also represent the toughness of the material [72]. It is not difficult to see that the rABS/rHIPS blends has the smallest stress-strain curve area. Moreover, the area of the

stress-strain curve increases gradually after the addition of SBG, which reflects the transition from brittle material to ductile material in the whole process.

The flexural strength of blends of rABS, rHIPS, and SBG is shown in Fig 9 (c). The blends' flexural strength tendency is essentially in line with their tensile strength trend that is reaching the maximum value when the SBG content is 2%. The reason for these changes may be that the PB phase in SBG, as an elastomer, has a poor tensile strength and flexural strength than the pure material system [73, 74]. However, the addition of epoxy groups still makes the tensile strength and flexural strength of the modified blends slightly higher than that before modification.

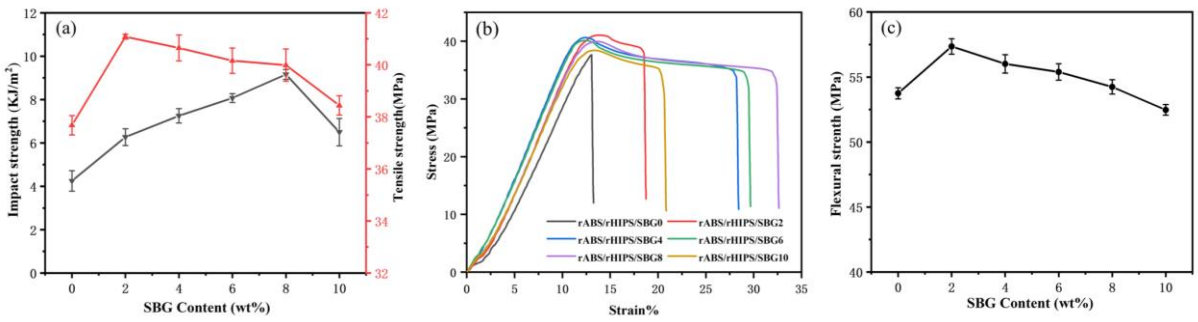

Fig. 9. Mechanical properties of rABS/rHIPS/SBG blends: (a)Impact strength and tensile strength; (b)Strain-stress curves; (c)Flexural strength.

3.9. Thermogravimetric analysis

The thermal stability of polymer materials is an important parameter to determine the properties of polymer materials [75]. **Fig. 10** is the TG and DTG curves of rABS/rHIPS/SBG blends. The initial decomposition temperature, 5% thermal weight loss temperature ($T_{5\%}$) and maximum weight loss temperature (T_{max}) can be obtained from the TG curve. Both $T_{5\%}$ and T_{max} of the blends are listed in **Table 5**. DTG curve is the first derivative of TG curve with respect to time, which

shows the relationship between temperature and mass change rate.. The temperature when the system reaches the maximum reaction rate can be obtained from the DTG curve, and the peak area of the DTG curve is proportional to the corresponding mass change of the sample. It can be seen from **Fig. 10** (a) demonstrates that the addition of SBG raises the initial decomposition temperature of rABS/rHIPS, 5% thermal weight loss temperature and maximum weight loss temperature, which proves that the thermal stability of the blends has been improved to a certain extent [76]. The peak value of the curve in **Fig. 10** (b) represents the temperature when the system reaches the maximum decomposition rate. The addition of SBG shifts the temperature of rABS/rHIPS to the high temperature region when the maximum decomposition rate is reached. This may be because the epoxy group in SBG reacts with the carboxyl group of aging group, repairing the broken molecular chains and increasing molecular entanglement. Thus, the thermal stability of the polymer is improved.

Table 5. TGA results of rABS/rHIPS/SBG blends.

Specimen	$T_{5\%}$ (℃)	T_{max} (℃)
rABS/rHIPS/SBG0	327.2	423.6
rABS/rHIPS/SBG2	340	427
rABS/rHIPS/SBG4	342.6	426.3
rABS/rHIPS/SBG6	334.5	427
rABS/rHIPS/SBG8	337.6	427.6
rABS/rHIPS/SBG10	337.8	427.6

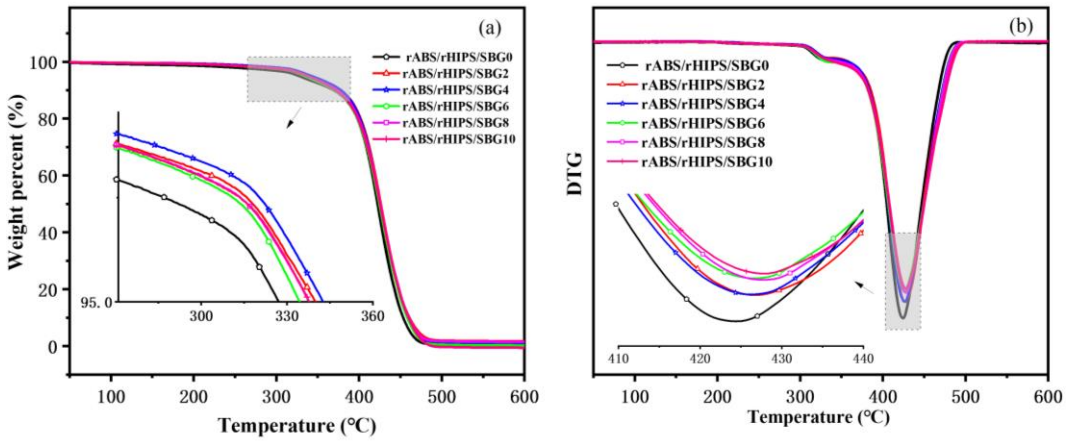

Fig. 10. TG (a) and DTG (b) curve of rABS/rHIPS/SBG blends.

3. Conclusions

This study is the first attempt to add SBG into the rABS/rHIPS system to improve the compatibility and performance of rABS/rHIPS. First, the FTIR spectra results revealed that ether bonds were created in the blends with SBG; second, the GPC results revealed an increase in the Mn and Mw of modified samples; and third, the MFI test result showed that the blends' flow performance deteriorated and their molecular entanglement levels rose as a result of the addition of SBG.. The above three experimental results indicated that epoxides in SBG react with carboxyl and hydroxyl groups in rABS/rHIPS. Then the rheological test results showed an increase in the storage modulus, loss modulus and complex viscosity of the adjusted samples; both DSC and DMA experiments proved that the glass transition temperatures of the two phases of the modified samples were close to each other; three fracture surfaces were tested by SEM and the results showed that the addition of SBG improved the compatibility of rABS and rHIPS, and the

toughness of the blends further improved with tthe addition of the rubber phase. The above four experiments successfully confirmed that the addition of SBG enhanced the compatibility of rABS/rHIPS. In addition, the test results of mechanical properties showed that the tensile strength, flexural strength and notched impact strength of the sample after adding SBG were improved, and the performance was the best when the content of SBG is 8%, the notched impact strength of the blends was 8.84 KJ/m^2, 2.08 times that of the original blends; TG test results showed that the temperature of the modified blends increases when it reaches the maximum decomposition rate. The aforementioned two experimental findings demonstrated that the inclusion of SBG enhanced the blends' mechanical and thermal stability. Above all, high-value recycling of rABS and rHIPS was ultimately accomplished through the introduction of SBG.

Acknowledgements

The authors acknowledge the financial support from Princess Nourah bint Abdularahman University Researchers Supporting Project number (PNURSP2023R18), Princess Nourah bint Abdularahman University, Riyadh, Saudi Arabia

References

[1] H. Kamat, C. Ch, r.R. Kini, S.B. Shenoy, Two-way Fluid Structure Interaction Analysis of Single Pad Externally Adjustable Fluid Film Bearing, Eng. Sci. 20 (2022) 352-363.

[2] A. Karthik, D.S. Chiniwar, M. Das, P.P. M, P. Prabhu, P.A. Mulimani, K. Samanth , N. Naik, Electric Propulsion for Fixed Wing Aircrafts - A Review on Classifications, Designs, and

Challenges, Eng. Sci. 16 (2021) 129-145.

[3] T. Kuang, S. Chen, Z. Gu, Z. Shen, A. Hejna, M.R. Saeb, F. Chen, M. Zhong, T. Liu, A facile approach to fabricate load-bearing porous polymer scaffolds for bone tissue engineering, Adv. Compos. Hybrid Mater. 5(2) (2022) 1376-1384.

[4] T. Kuang, M. Zhang, F. Chen, Y. Fei, J. Yang, M. Zhong, B. Wu, T. Liu, Creating poly(lactic acid)/carbon nanotubes/carbon black nanocomposites with high electrical conductivity and good mechanical properties by constructing a segregated double network with a low content of hybrid nanofiller, Adv. Compos. Hybrid Mater. 6(1) (2023) 48.

[5] J. Liu, E. Chen, Y. Wu, H. Yang, K. Huang, G. Chang, X. Pan, K. Huang, Z. He, M. Lei, Silver nanosheets doped polyvinyl alcohol hydrogel piezoresistive bifunctional sensor with a wide range and high resolution for human motion detection, Adv. Compos. Hybrid Mater. 5(2) (2022) 1196-1205.

[6] Y. Chen, J. Lin, G.A.M. Mersal, J. Zuo, J. Li, Q. Wang, Y. Feng, J. Liu, Z. Liu, B. Wang, B.B. Xu, Z. Guo, “Several birds with one stone” strategy of pH/thermoresponsive flame-retardant/photothermal bactericidal oil-absorbing material for recovering complex spilled oil, J. Mater. Sci. Technol. 128 (2022) 82-97.

[7] H.-y. Du, Y.-l. An, Y.-h. Wei, X.-d. Liu, L.-f. Hou, B.-s. Liu, M.-m. Liu, P.K. Liaw, Experimental and numerical studies on strength and ductility of gradient-structured iron plate obtained by surface mechanical-attrition treatment, Mater. Sci. Eng.: A 744 (2019) 471-480.

[8] S. Feng, F. Zhai, H. Su, D. Sridhar, H. Algadi, B.B. Xu, R.A. Pashameah, E. Alzahrani, H.M. Abo-Dief, Y. Ma, T. Li, Z. Guo, Progress of metal organic frameworks-based composites in electromagnetic wave absorption, Mater. Today. Phys. 30 (2023) 100950.

[9] C. Hou, W. Yang, H. Kimura, X. Xie, X. Zhang, X. Sun, Z. Yu, X. Yang, Y. Zhang, B. Wang, B.B. Xu, D. Sridhar, H. Algadi, Z. Guo, W. Du, Boosted lithium storage performance by local build-in electric field derived by oxygen vacancies in 3D holey N-doped carbon structure decorated with molybdenum dioxide, J.Mater.Sci.Technol. 142 (2023) 185-195.

[10] F. Li, Q. Li, H. Kimura, X. Xie, X. Zhang, N. Wu, X. Sun, B.B. Xu, H. Algadi, R.A. Pashameah, A.K. Alanazi, E. Alzahrani, H. Li, W. Du, Z. Guo, C. Hou, Morphology controllable urchin-shaped bimetallic nickel-cobalt oxide/carbon composites with enhanced electromagnetic wave absorption performance, J. Mater. Sci. Technol. 148 (2022) 250-259.

[11] D. Ping, F. Yi, G. Zhang, S. Wu, S. Fang, K. Hu, B.B. Xu, J. Ren, Z. Guo, NH4Cl-assisted preparation of single Ni sites anchored carbon nanosheet catalysts for highly efficient carbon dioxide electroreduction, J. Mater. Sci. Technol. 142 (2023) 1-9.

[12] Z. Wang, H. Zhu, N. Cao, R. Du, Y. Liu, G. Zhao, Superhydrophobic surfaces with excellent abrasion resistance based on benzoxazine/mesoporous SiO_2, Mater. Lett. 186 (2017) 274-278.

[13] H. Yin, W. Zhong, M. Yin, C. Kang, L. Shi, H. Tang, C. Yang, J.T. Althakafy, M. Huang, A.K. Alanazi, L. Qu, Y. Li, Carboxyl-functionalized poly(arylene ether nitrile)-based rare earth coordination polymer nanofibrous membrane for highly sensitive and selective sensing of Fe3+ ions, Adv. Compos. Hybrid Mater. 5(3) (2022) 2031-2041.

[14] H. Zhu, W. Hu, Y. Xu, B. Wang, D. Zheng, Y. Fu, C. Zhang, G. Zhao, Z. Wang, Gradient structure based dual-robust superhydrophobic surfaces with high-adhesive force, Appl. Surf. Sci. 463 (2019) 427-434.

[15] H. Zhu, W. Hu, S. Zhao, X. Zhang, L. Pei, G. Zhao, Z. Wang, Flexible and thermally stable superhydrophobic surface with excellent anti-corrosion behavior, J. Mater. Sci. 55(5) (2020) 2215-2225.

[16] S. Gao, X. Zhao, Q. Fu, T. Zhang, J. Zhu, F. Hou, J. Ni, C. Zhu, T. Li, Y. Wang, V. Murugadoss, G.A.M. Mersal, M.M. Ibrahim, Z.M. El-Bahy, M. Huang, Z. Guo, Highly transmitted silver nanowires-SWCNTs conductive flexible film by nested density structure and aluminum-doped zinc oxide capping layer for flexible amorphous silicon solar cells, J. Mater. Sci. Technol. 126 (2022) 152-160.

[17] Y. Guo, J. Xu, C. Lan, K. Bi, Broadband and High-efficiency Linear Polarization Converter Based on Reflective Metasurface, Eng. Sci. 14 (2021) 39-45.

[18] J. Lin, J. Li, S. Feng, C. Gu, H. Li, H. Lu, F. Hu, D. Pan, B.B. Xu, Z. Guo, An active bacterial anti-adhesion strategy based on directional transportation of bacterial droplets driven by triboelectric nanogenerators, Nano. Res. 16(1) (2023) 1052-1063.

[19] J. Liu, K. Liu, X. Pan, K. Bi, F. Zhou, P. Lu, M. Lei, A flexible semidry electrode for long-term, high-quality electrocardiogram monitoring, Adv. Compos. Hybrid. Mater. 6(1) (2022) 13.

[20] R. Wang, Z. Meng, X. Yan, T. Tian, M. Lei, R.A. Pashameah, H.M. Abo-Dief, H. Algadi, N.

Huang, Z. Guo, H. Tang, Tellurium intervened Fe-N codoped carbon for improved oxygen reduction reaction and high-performance Zn-air batteries, J. Mater. Sci. Technol. 137 (2023) 215-222.

[21] Y. Wu, J. Wu, Y. Lin, J. Liu, X. Pan, X. He, K. Bi, M. Lei, Melamine sponge skeleton loaded organic conductors for mechanical sensors with high sensitivity and high resolution, Adv. Compos. Hybrid. Mater. 6(1) (2022) 4.

[22] H. Yang, R. Shi, Q. Jiang, J. Ren, Properties and mechanism of two-way shape memory polyurethane composite under stress-free condition, Adv. Compos. Hybrid. Mater. 6(1) (2022) 1.

[23] H. Karimi-Maleh, Y. Orooji, F. Karimi, C. Karaman, Y. Vasseghian, E.N. Dragoi, O. Karaman, Integrated approaches for waste to biohydrogen using nanobiomediated towards low carbon bioeconomy, Adv. Compos. Hybrid. Mater. 6(1) (2022) 29.

[24] M. Kumari, G.R. Chaudhary, S. Chaudhary , A. Umar, Rapid Analysis of Trace Sulphite Ion Using Fluorescent Carbon Dots Produced from Single Use Plastic Cups, Eng. Sci. 17 (2022) 101-112.

[25] X. Meng, H. Yang, Z. Lu, Y. Liu, Study on catalytic pyrolysis and combustion characteristics of waste cable sheath with crosslinked polyethylene, Adv. Compos. Hybrid Mater. 5(4) (2022) 2948-2963.

[26] G. Qi, Y. Liu, L. Chen, P. Xie, D. Pan, Z. Shi, B. Quan, Y. Zhong, C. Liu, R. Fan, Z. Guo, Lightweight Fe3C@Fe/C nanocomposites derived from wasted cornstalks with high-efficiency

microwave absorption and ultrathin thickness, Adv. Compos. Hybrid Mater. 4(4) (2021) 1226-1238.

[27] D. Xu, G. Huang, L. Guo, Y. Chen, C. Ding, C. Liu, Enhancement of catalytic combustion and thermolysis for treating polyethylene plastic waste, Adv. Compos. Hybrid Mater. 5(1) (2022) 113-129.

[28] S. Nandy, S. Goswami, A. Marques, D. Gaspar, P. Grey, I. Cunha, D. Nunes, A. Pimentel, R. Igreja, P. Barquinha, L. Pereira, E. Fortunato, R. Martins, Cellulose: A Contribution for the Zero e-Waste Challenge, Adv. Mater. Technol-Us. 6(7) (2021).

[29] F. da Silva Müller Teixeira, A.C. de Carvalho Peres, T.S. Gomes, L.L.Y. Visconte, E.B.A.V. Pacheco, A Review on the Applicability of Life Cycle Assessment to Evaluate the Technical and Environmental Properties of Waste Electrical and Electronic Equipment, J. Polym. Environ. 29(5) (2020) 1333-1349.

[30] C. Jia, P. Das, I. Kim, Y.-J. Yoon, C.Y. Tay, J.-M. Lee, Applications, treatments, and reuse of plastics from electrical and electronic equipment, J. Ind. Eng. Chem. 110 (2022) 84-99.

[31] S. Vishwakarma, V. Kumar, S. Arya, M. Tembhare, Rahul, D. Dutta, S. Kumar, E-waste in Information and Communication Technology Sector: Existing scenario, management schemes and initiatives, Environ. Technol. Inno. 27 (2022).

[32] Z. Wang, H. Jiang, Y. Zhang, K. Bian, H. Wang, C. Wang, Stepwise flotation separation of WEEE plastics by polymeric aluminum chloride towards source control of microplastics, Waste.

Manag. 149 (2022) 1-10.

[33] D. Hirayama, C. Saron, Morphologic and mechanical properties of blends from recycled acrylonitrile-butadiene-styrene and high-impact polystyrene, Polymer 135 (2018) 271-278.

[34] E. Maris, P. Botané, P. Wavrer, D. Froelich, Characterizing plastics originating from WEEE: A case study in France, Miner. Eng. 76 (2015) 28-37.

[35] G. Martinho, A. Pires, L. Saraiva, R. Ribeiro, Composition of plastics from waste electrical and electronic equipment (WEEE) by direct sampling, Waste. Manag. 32(6) (2012) 1213-7.

[36] M. Schlummer, L. Gruber, A. Maurer, G. Wolz, R. van Eldik, Characterisation of polymer fractions from waste electrical and electronic equipment (WEEE) and implications for waste management, Chemosphere. 67(9) (2007) 1866-76.

[37] S.K. Utimura, A.P. Chaves, J.A.S. Tenório, D.C.R. Espinosa, Selecting chemicals for separation of ABS and HIPS in WEEE by froth flotation, Polímeros. 29(2) (2019) e2019017.

[38] I. Hamarat, E. Kuram, B. Ozcelik, Investigation the mechanical, rheological, and morphological properties of acrylonitrile butadiene styrene blends with different recycling number content, J. Process Mechanical Eng. 232(4) (2017) 449-458.

[39] Z. Zhan, H. He, Z. Zhu, B. Xue, G. Wang, M. Chen, C. Xiong, Blends of rABS and SEBS: Influence of In-Situ Compatibilization on the Mechanical Properties, Materials 12(15) (2019) 2352.

[40] T. Chen, J. Zhang, Compatibilization of acrylonitrile-butadiene-styrene terpolymer/poly(ethylene glycol-co-1,4-cyclohexanedimethanol terephthalate) blend: effect on

morphology, interface, mechanical properties and hydrophilicity, Appl. Surf. Sci. 437 (2018) 62-69.

[41] Y. Li, X. Wu, J. Song, J. Li, Q. Shao, N. Cao, N. Lu, Z. Guo, Reparation of recycled acrylonitrile- butadiene-styrene by pyromellitic dianhydride: Reparation performance evaluation and property analysis, Polymer 124 (2017) 41-47.

[42] Z. Zhang, M. Liu, M.M. Ibrahim, H. Wu, Y. Wu, Y. Li, G.A.M. Mersal, I.H. El Azab, S.M. El-Bahy, M. Huang, Y. Jiang, G. Liang, P. Xie, C. Liu, Flexible polystyrene/graphene composites with epsilon-near-zero properties, Adv. Compos. Hybrid. Mater. 5(2) (2022) 1054-1066.

[43] Y. Kong, Y. Li, G. Hu, N. Cao, Y. Ling, D. Pan, Q. Shao, Z. Guo, Effects of polystyrene-b-poly(ethylene/propylene)-b-polystyrene compatibilizer on the recycled polypropylene and recycled high-impact polystyrene blends, Polym. Adv. Technol. 29(8) (2018) 2344-2351.

[44] Y.V. Vazquez, S.E. Barbosa, Process Window for Direct Recycling of Acrylonitrile-Butadiene-Styrene and High-Impact Polystyrene from Electrical and Electronic Equipment Waste, Waste. Manag. 59 (2017) 403-408.

[45] Y. Li, S. Jia, S. Du, Y. Wang, L. Lv, J. Zhang, Improved properties of recycled polypropylene by introducing the long chain branched structure through reactive extrusion, Waste. Manag. 76 (2018) 172-179.

[46] J. Li, F. Chen, L. Yang, L. Jiang, Y. Dan, FTIR analysis on aging characteristics of ABS/PC blend under UV-irradiation in air, Spectrochim. Acta. A. 184 (2017) 361-367.

[47] D. Salari, H. Ranjbar, Study on the recycling of ABS resins: Simulation of reprocessing and thermo-oxidation, Iran. Polym. J. 17(8) (2008) 599-610.

[48] P. Davis, The effect of photo-oxidative degradation on fracture in ABS pipe resins, Polym. Degradation Stab. 84(2) (2004) 233-242.

[49] R. Fiorio, S. Villanueva Diez, A. Sanchez, R. D'Hooge D, L. Cardon, Influence of Different Stabilization Systems and Multiple Ultraviolet A (UVA) Aging/Recycling Steps on Physicochemical, Mechanical, Colorimetric, and Thermal-Oxidative Properties of ABS, Materials 13(1) (2020) 212.

[50] G. Iannuzzi, B. Mattsson, M. Rigdahl, Color changes due to thermal ageing and artificial weathering of pigmented and textured ABS, Polym. Eng. Sci. 53(8) (2013) 1687-1695.

[51] J. Wang, Y. Li, J. Song, M. He, J. Song, K. Xia, Recycling of acrylonitrile–butadiene–styrene (ABS) copolymers from waste electrical and electronic equipment (WEEE), through using an epoxy-based chain extender, Polym. Degradation Stab. 112 (2015) 167-174.

[52] B. Qiao, G.S. Hu, M.Y. He, Y.C. Li, Reactive Compatibilization of Recycled HIPS/ABS Blends with Maleic-Anhydride Grafted Styrene-Ethylene-Butadiene-Styrene and Oxazoline-Modified Recycled ABS, Oxid. Commun. 39(2A) (2016) 2085-2100.

[53] Y. Cui, Y. Li, W. Wang, X. Wang, J. Lin, X. Mai, G. Song, N. Naik, Z. Guo, Flotation separation of acrylonitrile-butadienestyrene (ABS) and high impact polystyrene (HIPS) from waste electrical and electronic equipment (WEEE) by potassium permanganate surface

modification, Sep. Purif. Technol. 269 (2021).

[54] D. Hirayama, L.A. Nunnenkamp, F.H.G. Braga, C. Saron, Enhanced mechanical properties of recycled blends acrylonitrile–butadiene–styrene/high–impact polystyrene from waste electrical and electronic equipment using compatibilizers and virgin polymers, J. Appl. Polym. Sci. 139(13) (2021) 51873.

[55] Y.V. Vazquez, S.E. Barbosa, Compatibilization of HIPS/ABS blends from WEEE by using Styrene-Butadiene Rubber (SBR), J Environ Manage 217 (2018) 381-390.

[56] Y. Wang, Y. Li, W. Wang, L. Lv, C. Li, J. Zhang, Recycled polycarbonate/acrylonitrile-butadiene-styrene reinforced and toughened through chemical compatibilization, J. Appl. Polym. Sci. 136(21) (2019) 47537.

[57] Y. Pan, G. Wu, H. Ma, S. Zhou, H. Zhang, Improved compatibility of PET/HDPE blend by using GMA grafted thermoplastic elastomer, Polym-Plast. Tech. Mat. 59(17) (2020) 1887-1898.

[58] S. Sun, M. Zhang, H. Zhang, X. Zhang, Polylactide toughening with epoxy-functionalized grafted acrylonitrile-butadiene-styrene particles, J. Appl. Polym. Sci. 122(5) (2011) 2992-2999.

[59] Z.Y. Tan, S.C. Liu, X.L. Cui, S.L. Sun, H.X. Zhang, Application of macromolecular chain extender and contribution to the toughening of poly(ethylene terephthalate), J. Thermoplast. Compos. Mater. 29(6) (2016) 833-849.

[60] X. Liu, A. Boldizar, M. Rigdahl, H. Bertilsson, Recycling of blends of acrylonitrile-butadiene-styrene (ABS) and polyamide, J. Appl. Polym. Sci. 86(10) (2002) 2535-2543.

[61] L. Shu, Y. Li, J. Li, W. Wang, S. Vupputuri, D. Yang, B. Dong, N. Cao, D. Pan, R. Das, Z. Guo, Chain Extension, Phase Interface Reparation and Mechanical Property of Recycled Acrylonitrile-Butadiene-Styrene by Epoxidized Styrene-Butadiene-Styrene, Macromol. Mater. Eng. 305(11) (2020) 2000284.

[62] X. Dong, M. Dong, Y. Li, Z. Li, W. Wang, N. Cao, K.H. Mahmoud, S.M. El-Bahy, Z.M. El-Bahy, M. Huang, Z. Guo, Building blend from recycling acrylonitrile–butadiene–styrene and high impact-resistance polystyrene through dextro-glucose, React. Funct. Polym. 175 (2022) 105287.

[63] A. Mojarrad, A. Ramazani SA, I. Ghasemi, A. Vaziri, Rheological and morphological behaviors of polyamide 6/acrylonitrile–butadiene–styrene/nanoclay nanocomposites, J. Thermoplast. Compos. Mater. 27(10) (2014) 1399-1416.

[64] H. Essabir, F.Z. El Mechtali, S. Nekhlaoui, M. Raji, M.O. Bensalah, D. Rodrigue, R. Bouhfid, A. Qaiss, Compatibilization of PA6/ABS blend by SEBS-g-MA: morphological, mechanical, thermal, and rheological properties, Int. J. Adv. Manuf. Tech. 110(3-4) (2020) 1095-1111.

[65] B. Chang, Y. Li, W. Wang, G. Song, J. Lin, V. Murugadoss, N. Naik, Z. Guo, Impacts of chain extenders on thermal property, degradation, and rheological performance of poly(butylene adipate-co-terephthalate), J. Mater. Res. 36(15) (2021) 3134-3144.

[66] Y. Lyu, Y. Chen, Z. Lin, J. Zhang, X. Shi, Manipulating phase structure of biodegradable PLA/PBAT system: Effects on dynamic rheological responses and 3D printing, Compos. Sci. Technol. 200 (2020).

[67] M.A. Sohel, A. Mandal, A. Mondal, S. Pan, A. SenGupta, Thermal analysis of ABS/PA6 polymer blend using differential scanning calorimetry, J. Therm. Anal. Calorim. 129(3) (2017) 1689-1695.

[68] Z.N. Yin, L.F. Fan, T.J. Wang, Experimental investigation of the viscoelastic deformation of PC, ABS and PC/ABS alloys, Mater. Lett. 62(17-18) (2008) 2750-2753.

[69] F. Wang, R.Y. Hong, W.G. Feng, D. Badami, K. Zeng, Electrical and mechanical properties of ABS/EPDM composites filled with carbon black, Mater. Lett. 125 (2014) 48-50.

[70] D. Ye, S. Li, X. Lu, X. Zhang, O.J. Rojas, Antioxidant and Thermal Stabilization of Polypropylene by Addition of Butylated Lignin at Low Loadings, Acs. Sustain. Chem. Eng. 4(10) (2016) 5248-5257.

[71] M.N. Machmud, M. Omiya, H. Inoue, K. Kishimoto, Impact-induced fracture mechanisms of immiscible PC/ABS (50/50) blends, IOP. Conf. S. Mat. Sci. Eng. 334 (2018) 012078.

[72] F. Liu, Y. Yan, L. Li, C. Lan, G. Chen, Performance of Recycled Plastic-Based Concrete, J. Mater. Civ. Eng., 27 (2) (2013), p. A4014004.

[73] Y.V. Vazquez, S.E. Barbosa, Compatibilization Strategies for Recycling Applications of High Impact Polystyrene/Acrylonitrile Butadiene Blends, J. Polym. Environ. 25(3) (2016) 903-912.

[74] M.A. Peydro Rasero, F.P. Garcia, R. Navarro Vidal, J.E. Crespo Amoros, Influence of styrene–ethylene–butylene–styrene on the properties of acrylonitrile butadiene styrene–high-impact polystyrene blends, J. Elastom. Plast. 47(5) (2013) 449-462.

[75] S. Bano, N. Ramzan, T. Iqbal, H. Mahmood, F. Saeed, Study of thermal degradation behavior and kinetics of ABS/PC blend, Pol. J. Chem. Technol. 22(3) (2020) 64-69.

[76] J. Andrzejewski, A.K. Mohanty, M. Misra, Development of hybrid composites reinforced with biocarbon/carbon fiber system. The comparative study for PC, ABS and PC/ABS based materials, Compos. Part. B-Eng. 200 (2020).